

DOI: 10.1002/cplu.201300439

 **A Metal-Free, Carbon-Based Catalytic System for the Oxidation of Lignin Model Compounds and Lignin**Yongjun Gao,<sup>[a]</sup> Jianguang Zhang,<sup>[a]</sup> Xi Chen,<sup>[a]</sup> Ding Ma,<sup>[b]</sup> and Ning Yan<sup>\*[a]</sup>

Nitrogen-containing graphene material (LCN) has been identified as an effective catalyst for the oxidation of  $\beta$ -O-4 and  $\alpha$ -O-4 types of lignin model compounds in the presence of *tert*-butyl hydroperoxide, to provide aromatic aldehydes, acids and other organic chemicals in high yield. The transformations of five lignin model compounds over LCN were investigated systematically. Instrumentation analysis, kinetic study and radical trapping experiments highlight the mechanistic features of the reaction, including: 1) the reaction pathway starts by benzylic C–H or C–OH bond activation, followed by  $C_{\alpha}$ – $C_{\beta}$  or  $C_{\alpha}$ –O

bond cleavage, and finally further oxidation of intermediate aromatics; and 2) the reaction follows a free-radical mechanism with all the key steps involving radical species. In addition, the LCN proved to be a highly stable catalyst; no significant activity decrease was observed for four consecutive runs, and X-ray photoelectron spectroscopy analysis indicates negligible decrease in the content of the active nitrogen species in the catalyst. Notably, this new catalytic system can be extended to the oxidative depolymerisation of real lignin, to produce a significant portion of liquefied, low-molecular-mass products.

**Introduction**

It is not unreasonable to speculate that biomass, such as cellulose, lignin, even chitin, would be the major source for certain fine chemicals or platform compounds in the post-fossil fuel era.<sup>[1]</sup> Among various biomass materials, lignin could be seen as the major resource for sustainable aromatic chemicals, because lignin is the most abundant, renewable aromatic biopolymer on earth.<sup>[2]</sup> There are three major strategies to depolymerise lignin into an array of simple compounds: hydrogenolysis,<sup>[3]</sup> hydrolysis<sup>[4]</sup> and oxidation.<sup>[5]</sup> Among these, the oxidative depolymerisation of lignin is unique because it leads to highly functionalised monomeric or oligomeric products, which can be used directly as fine chemicals or as platform chemicals.<sup>[5c,6]</sup>

It has long since been established that lignin has a complex, mildly branched polymeric structure composed of a few aromatic monomers randomly coupled and cross-coupled by C–O or C–C bonds. The C–O bond is the major linkage among the monomers, with  $\beta$ -O-4,  $\alpha$ -O-4 and 4-O-5 linkages being most representative. The C–C bond contributes a minor fraction (about a third) to the linkages in lignin.<sup>[7]</sup> To generate commodity chemicals from lignin, these linkages have to be broken down. Under oxidative conditions, the benzylic C–H or

C–OH bonds in lignin can be attacked relatively easily and transformed to carbonyl groups. Then the  $C_{\alpha}$ –O or  $C_{\alpha}$ – $C_{\beta}$  bond undergoes cleavage to afford depolymerised products.<sup>[5c]</sup> The key to achieving the selective oxidation of lignin into chemicals relies on the development of appropriate catalysis technologies. The oxidation of lignin and associated model compounds has been studied extensively.<sup>[2d,5c]</sup> A vast majority of reported oxidative catalytic systems are based on using metal-containing catalysts, and many of them suffer from low efficiency, harsh reaction conditions and/or use toxic metals.<sup>[7a,8]</sup> Recently, a metal-free catalytic system consisting of 4-acetamido-TEMPO (TEMPO = 2,2,6,6-tetramethyl-1-piperidinyl-oxo) in combination with  $\text{HNO}_3$  and HCl was developed to catalyse the oxidation of benzylic alcohol as a lignin model compound.<sup>[9]</sup> Nevertheless, efficient, metal-free catalytic systems for the oxidation of lignin model compounds and real lignin remain very limited. Also, the reaction pathway and the reaction mechanism of lignin oxidation in metal-free catalytic systems remain elusive.

In this work, systematic evaluation of the oxidation of various lignin model compounds over nitrogen-containing graphene material (LCN) in the presence of organic peroxides was conducted. Detailed product identification, kinetic study and free-radical trapping experiments highlight the salient mechanistic features of this new catalytic oxidation system for lignin conversion. To our delight, this carbon-based catalytic system is even able to transform organosolv lignin, which leads to a significant portion of liquefied, partially depolymerised products. The depolymerised products can be further hydrolysed to low-molecular-weight compounds, such as diethyl succinate and diethyl phthalate, in acidic ethanol–water solution.

[a] Dr. Y. Gao, J. Zhang, X. Chen, Prof. N. Yan  
Department of Chemical and Biomolecular Engineering  
National University of Singapore  
4 Engineering Drive 4, 117576 Singapore (Singapore)  
E-mail: ning.yan@nus.edu.sg

[b] Prof. D. Ma  
Beijing National Laboratory for Molecular Sciences  
College of Chemistry and Molecular Engineering  
Peking University, 202 Chenfu Road, Beijing 100871 (P. R. China)

 Supporting information for this article is available on the WWW under <http://dx.doi.org/10.1002/cplu.201300439>.

 This article is part of the "Early Career Series". To view the complete series, visit: <http://chempluschem.org/earlycareer>.

## Results and Discussion

### LCN characterisation

Compared with normal graphene material, the exceptional catalytic performance of LCN originates from its nitrogen doping.<sup>[10]</sup> Therefore, the LCN in this study was prepared by following a modified literature method by using chemical vapour deposition (CVD) with pyrolytic graphene oxide as substrate and acetonitrile as nitrogen source, in which the nitrogen content of LCN was maximised by elongated exposure to acetonitrile.<sup>[10]</sup> The synthesised LCN can be regarded as a nitrogen-containing, layered carbon material possessing highly exfoliated graphitic structures. Transmission electron microscopy (TEM) and scanning electron microscopy (SEM) analysis (see Figure 1 a,b) clearly show that the LCN possesses a graphitic sheet structure. X-ray photoelectron spectroscopy (XPS; see Figure 1 c) exhibits only three sets of peaks, at around 284.8, 401.5 and 531.8 eV, corresponding to carbon, nitrogen and oxygen, respectively. Based on XPS analysis, the nitrogen content in the LCN we used was 6.2 wt%, which is similar to that of LCNs exhibiting excellent catalytic activity in the literature.<sup>[10]</sup> Fitting results of the N1s XPS spectrum are shown in Figure 1 d. The peaks at 398.6, 399.6, 401.5 and 403.5 eV are assigned to pyridinic N, pyrrolic N, graphitic N and oxidised N, respectively.<sup>[11]</sup> Among these four nitrogen species, graphitic N,

which according to DFT calculations<sup>[10]</sup> is responsible for the catalytic activity of LCN, is the major constituent (58% according to XPS fitting results). Overall, the synthesised LCN in this study shows a graphene-based sheet structure containing catalytically active, graphitic N species (> 3 wt%).

### Oxidation of lignin model compounds

Both the  $\alpha$ -O-4 and the  $\beta$ -O-4 types of lignin model compounds contain the benzylic C–H or C–OH bond. As such, our strategy for lignin conversion is to utilise LCN as a catalyst to activate the benzylic C–H or C–OH bond in the presence of an oxidant. Previous works on the oxidation of lignin and its model compounds employed oxygen and/or H<sub>2</sub>O<sub>2</sub> as oxidant owing to their low price.<sup>[5a,b,12]</sup> Our preliminary data (Table 1, entry 1), however, indicated that H<sub>2</sub>O<sub>2</sub> is not suitable in the LCN-catalysed oxidation of lignin model compounds, presumably because of the fast decomposition of H<sub>2</sub>O<sub>2</sub> under the applied conditions.

Therefore, *tert*-butyl hydroperoxide (TBHP), which is a more stable oxidant widely used in industrial processes, was chosen for further study. We started the work by evaluating the performance of LCN in the oxidation of lignin model compounds in the presence of TBHP. 1-(Benzyloxy)-2-methoxybenzene (**a**; see Table 1) and benzyl phenyl ether (**b**) were selected as  $\alpha$ -O-4 type model compounds whereas 2-phenoxy-1-phenylethanol (**c**), 2-(2,6-dimethoxyphenoxy)-1-phenylethanol (**d**) and 2-(2,6-dimethoxyphenoxy)-1-phenylethanol (**e**) were selected as  $\beta$ -O-4 type lignin model compounds. Both  $\alpha$ -O-4 and  $\beta$ -O-4 types of model compounds contain two benzene rings. For clarity, the benzene ring directly connected with a carbon atom, that is, the ring associating with the benzylic C–H or C–OH bonds, is denoted as the A ring, whereas the benzene ring directly connected with an oxygen atom is denoted as the B ring.

The results of the catalytic oxidation of  $\alpha$ -O-4 type model compounds (**a**, **b**) over LCN are compiled in Table 1. Only small amounts of benzaldehyde **1** (0.6 mol%) and 2-methoxyphenol **3** (0.2 mol%) were formed in the blank experiment (Table 1, entry 2), whereas noticeable conversion and yield were achieved by employing LCN as a catalyst. As mentioned, the conversion of compound **a** and the yields of aromatic products were low when H<sub>2</sub>O<sub>2</sub> was used as the oxi-

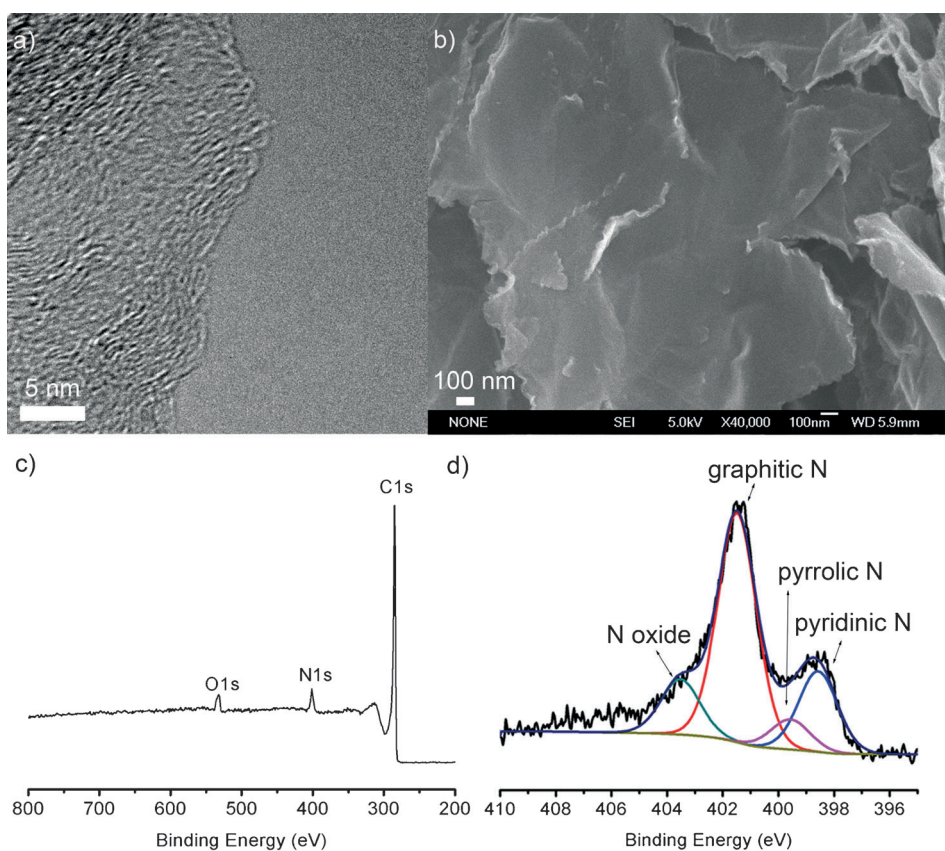
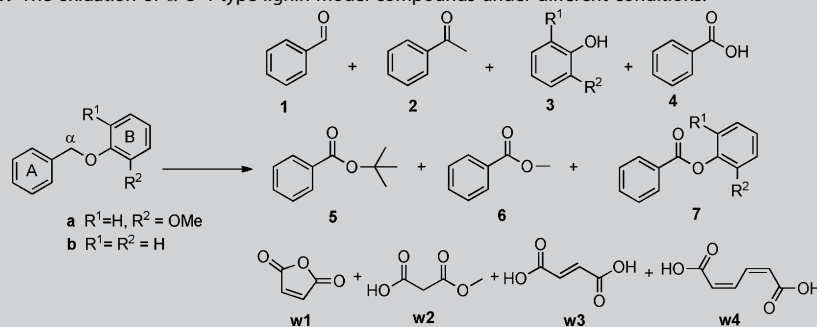


**Figure 1.** a) TEM and b) SEM images of LCN material; c) XPS spectrum and d) XPS N 1s spectrum of LCN.

**Table 1.** The oxidation of  $\alpha$ -O-4 type lignin model compounds under different conditions.<sup>[a]</sup>



Entry	Substrate	Conversion [%]	Total yield [mol%]	Yield [mol%]						
				1	2	3	4	5	6	7
1 <sup>[b]</sup>	a	25.0	9.1	2.5	4.1	2.2	0	0	0	0.3
2 <sup>[c]</sup>	a	9.0	0.8	0.6	0	0.2	0	0	0	0
3 <sup>[d]</sup>	a	40.1	25.9	15.9	2.0	2.9	2.2	0.08	0	2.8
4	a	66.5	41.9	14.5	1.9	1.4	21.0	0.5	0	2.6
5 <sup>[e]</sup>	a	89.4	57.0	5.6	2.7	1.5	40.6	1.7	0	4.9
6 <sup>[f]</sup>	a	98.0	71.0, 7.2 (w1)	3.0	1.5, 0.8 (w2)	0.9	45.5, 0.3 (w3)	1.4	0.4, 0.7 (w4)	9.3
7 <sup>[g]</sup>	a	85.4	54.9	6.9	2.4	1.5	40.4	0.6	0.1	3.0
8 <sup>[e]</sup>	b	68.6	74.2	13.2	2.9	19.0	33.7	0.5	-	4.9

[a] Reaction conditions: substrate (0.5 mmol), LCN (0.01 g), TBHP (6 equiv, 70 wt% in water), H<sub>2</sub>O (3 mL), 80 °C, 12 h. The conversion and yield were determined by GC analysis (only organic-phase products were quantified). [b] H<sub>2</sub>O<sub>2</sub> (20 equiv) was used as oxidant. [c] No catalyst was used. [d] 3 equiv TBHP. [e] Reaction time is 24 h. [f] 12 equiv TBHP was used and the yields of compounds in the water phase (w1–w4) were quantified. [g] Reaction temperature 120 °C.

dant, even if H<sub>2</sub>O<sub>2</sub> was used in a large excess (20 equiv; Table 1, entry 1). TBHP, on the other hand, exhibited superior oxidative ability under similar reaction conditions. Three equivalents of TBHP at 80 °C led to 40% conversion with a variety of aromatic chemicals detected (Table 1, entry 3). The conversion of **a** further increases on increasing the amount of TBHP, reaction temperature and/or reaction time (Table 1, entries 3–7). The catalytic system is also applicable with model compound **b**, affording comparable substrate conversion and product yield (Table 1, entry 8). After the reaction, seven aromatic compounds (1–7) were identified, with benzaldehyde **1** and benzoic acid **4** as the major products. Products 1–6 are mono-aromatic compounds formed by oxidative C<sub>α</sub>–O bond cleavage, which highlights that LCN is an effective catalyst for the oxidative decoupling of  $\alpha$ -O-4 type lignin model compounds using TBHP as an oxidant. Product **7**, which is generated by benzylic C–H bond oxidation without C–O bond cleavage, was also detected but in a small amount.

A close examination revealed that the mono-aromatic products (1, 2, 4–6) are generated from the A ring whereas **3** is generated from the B ring. In principle, the combined yield of the products from the A ring should equal that of the products from the B ring. However, the yield of **3** (2-methoxyphenol in this case) was significantly lower than the combined yield of 1, 2 and 4–6, which suggests that product(s) from the B ring underwent further transformation into polar, non-aromatic compounds. These chemicals stay preferentially in the water phase upon organic solvent extraction (note that ethyl acetate was

employed to extract the products from water) and escape GC and GC–MS analysis. To verify this assumption, the water phase after extraction was freeze-dried and analysed by GC–MS (see Figure S1 in the Supporting Information). Indeed, a variety of dicarboxylic acids and their derivatives, such as oxalic acid, maleic anhydride, maleic acid, fumaric acid and muconic acid, were detected. In a following experiment, 2-methoxyphenol **3** was used as the substrate instead of **a** under the same reaction conditions. No 2-methoxyphenol survived after the reaction. These results demonstrated that the 2-methoxyphenol generated from the B ring is further oxidised into water-soluble chemicals through a series of reactions. The first step is likely to be similar to the reported Malaprade reaction, in which *o*-quinone and methanol are generated from 2-methoxyphenol and an oxidant.<sup>[13]</sup> Fol-

lowing that, the *o*-quinone reacts with TBHP to form muconic acid, which is further oxidised to other dicarboxylic acids (Figure S2). Quantitative analysis of one experiment indicates a combined yield of approximately 10 mol% for water-soluble products, including maleic anhydride (w1, 7.2 mol%), hexadienoic acid (w4, 0.7 mol%) and two others (Table 1, entry 6).

The tendency for over-oxidation of the B ring product(s) into dicarboxylic acids and their derivatives is closely related to the nature of the substituent groups (R<sub>1</sub> and R<sub>2</sub>). Starting from **b** (R<sub>1</sub>=R<sub>2</sub>=H), the yield of phenol (product from the B ring) reaches 19.0 mol%, which indicates that the *ortho*-methoxy group enables the molecule to be more susceptible towards over-oxidation owing to the electron-donating property of the methoxy group.

The LCN-catalysed oxidations of lignin  $\beta$ -O-4 model compounds (**c**–**e**) were also investigated (Table 2). Compound **c** was selected for reaction condition optimisation. Not surprisingly, no reaction occurred without adding LCN. At 80 °C for 12 hours, the conversion of **c** reaches 69.3% in the presence of LCN. The major product is ketone ether **11** generated from the oxidation of the benzylic C–OH bond without C–O or C–C bond cleavage. Benzoic acid **4** was obtained as the dominant monomer along with other monomeric products, such as phenyl formate **8** and phenol **3** (Table 2, entry 1). Notably, the fact that **4** was the major product from the A ring indicates that the major reaction pathway involves C<sub>α</sub>–C<sub>β</sub> bond cleavage, which is further corroborated by the existence of **8** in the product. An increase in the reaction time to 24 hours led to an

**Table 2.** The oxidation of  $\beta$ -O-4 type lignin model compounds under different conditions.<sup>[a]</sup>

c R<sup>1</sup> = R<sup>2</sup> = H  
d R<sup>1</sup> = H, R<sup>2</sup> = OMe  
e R<sup>1</sup> = R<sup>2</sup> = OMe

Entry	Substrate	T [°C]	t [h]	Conversion [%]	Total yield [mol %]	Yield [mol %]									
						1	2	3	4	5	8	9	10	11	
1	c	80	12	69.3	68.7	0.1	0.6	1.0	16.0	4.6	0.4	0.7	1.0	44.3	
2	c	80	24	88.0	73.5	0.2	1.2	3.1	24.5	3.3	0.3	0.2	3.1	37.6	
3	c	120	24	91.8	97.4	0.2	2.1	18.3	45.3	2.0	0.2	0.3	18.3	10.7	
4	d	120	24	95.8	62.7	0.1	4.3	5.1	42.4	0.5	0	0	0	10.3	
5	e	120	24	quant.	72.9	0.1	8.7	0	33.5	0	0	14.6	0	16.0	

[a] Reaction conditions: substrate (0.5 mmol), LCN (0.01 g), TBHP (6 equiv, 70 wt% in water), H<sub>2</sub>O (3 mL). The conversion and yield were determined by GC analysis (only organic-phase products were quantified). quant. = quantitative.

tions. As shown in Figure 2a, the initial reaction rate of **a** is high, reaching 53% conversion after 3 hours. Afterwards, the conversion keeps increasing smoothly. Compounds **1**, **3** (R<sub>1</sub> = H, R<sub>2</sub> = OMe), **4** and **7** (R<sub>1</sub> = H, R<sub>2</sub> = OMe) are the major products, and they exhibit very interesting selectivity changes as the reaction evolves. The yield of the dimeric product **7** (R<sub>1</sub> = H, R<sub>2</sub> = OMe) reaches its maximum at *t* = 1 h and drops afterwards. The yields of monomeric products **1** and **3** increase in the first 3 and 0.5 hours, respectively, and then decrease. On the contrary, the yield of **4** keeps increasing during the entire process. These

increased conversion of **c** and increased yield of monomers, but **11** remained as the major product. By increasing the reaction temperature to 120 °C, C<sub>α</sub>-C<sub>β</sub> bond cleavage is significantly promoted: the A ring is mainly converted into **4** (45.3 mol%) whereas the B ring is mainly converted into **3** (18.3 mol%) and **10** (18.3 mol%) monomers (Table 2, entry 3).

Two other  $\beta$ -O-4 type lignin model compounds, **d** and **e**, were also converted into monomeric compounds with satisfactory yield under optimised conditions (Table 2, entries 4 and 5).

The major difference is that the yields for the major products from the B ring, that is, compounds **3** and **10**, are considerably lower. This result is in full agreement with the observations of the LCN-catalysed  $\alpha$ -O-4 type model compound conversion, in which we identified that the *ortho*-methoxy substituents decrease the stability of the aromatic ring significantly. The experiments shown in Table 2 demonstrate effective catalytic oxidation of  $\beta$ -O-4 type lignin model compounds in the presence of LCN and TBHP, despite the fact that a slightly higher temperature is required to achieve reasonable monomer yields.

### Kinetics and reaction mechanism

Kinetic studies on the oxidation of compounds **a** and **c** over LCN in a period of 24 hours at 80 °C were conducted (see Figure 2 and detailed data in Table S1). In both cases, no significant drop in activity was observed in the entire period, thus indicating that LCN remains active under these reaction condi-

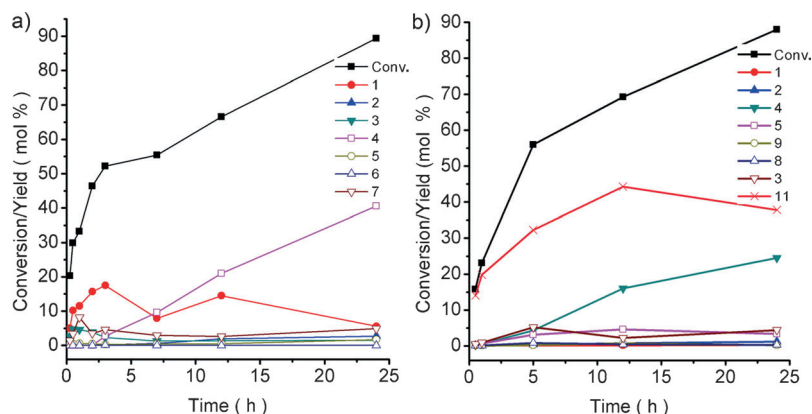


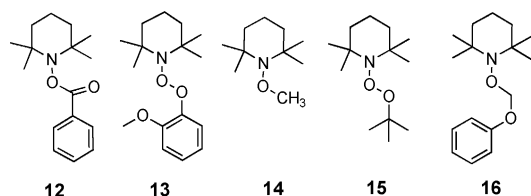
**Figure 2.** Product distributions for the conversion of a) **a** and b) **c** over LCN as functions of time. Reaction conditions: substrate (0.5 mmol), TBHP (6.0 mmol, 70 wt% in water), LCN (0.01 g), H<sub>2</sub>O (3 mL), 80 °C; the conversion and yield were determined by GC.

results suggest that the oxidative decoupling of **a** over LCN first occurs at the position of the benzylic C-H bond to generate dimeric product **7** (R<sub>1</sub> = H, R<sub>2</sub> = OMe). Cleavage of **7** at the position of C<sub>α</sub>-O generates products **1** and **3** (R<sub>1</sub> = H, R<sub>2</sub> = OMe). Product **1** is further oxidised into its acid form **4**, which is a stable end product. Product **3** is highly unstable under the applied conditions and is decomposed, in agreement with the observation of dicarboxylic acids and associated derivatives after the reaction.

Kinetic study employing **c** as the substrate provides similar information (Figure 2b). Compound **c** was converted smoothly. The dimeric product **11** (R<sub>1</sub> = R<sub>2</sub> = H) is the main product within the first 12 hours, which indicates that the reaction starts from the oxidation of the benzylic C-OH bond. Following that, the decomposition of **11** (R<sub>1</sub> = R<sub>2</sub> = H) leads to the formation of aromatic monomers, which is the rate-determining step in this case. Similar to **a**, **4** is the stable end product after oxidation of **c** via **1** as an intermediate.

A vast majority of catalytic systems for lignin oxidation involve free radicals during the reaction.<sup>[5c]</sup> It is also widely reported that TBHP acts as a free-radical initiator, either generating *tert*-butoxide and hydroxyl radicals under microwave irradiation<sup>[6a]</sup> or reacting with metal catalysts to form *tert*-butylperoxy radicals.<sup>[3g]</sup> As such, it is not unreasonable to speculate that LCN-catalysed lignin model compound oxidation in the presence of TBHP follows a free-radical mechanism. To identify the radical species produced during the reaction, radical trapping experiments with TEMPO as a radical scavenger were conducted. Compounds **a** and **c** were used as substrates and TEMPO was added into the system 5–10 minutes after the reaction to trap the active intermediate species.

Employing **a** as the substrate, four TEMPO adducts, denoted as **12**, **13**, **14** and **15** (see Scheme 1 and Figure S3), were detected by GC–MS, thus demonstrating the formation of at least four radical species during the reaction. Benzoyl radicals and 2-methoxyphenoxy radicals are derived from the A and B rings



**Scheme 1.** The TEMPO adducts detected by GC–MS in the radical trapping experiment using **a** and **c** as the substrates.

of the substrate, respectively (trapped as **12**, **13**), and methyl radicals and *tert*-butoxyl radicals are formed from TBHP (trapped as **14**, **15**). By combining the kinetic study, the radical trapping experiments and the previous literature reports,<sup>[3g,6a]</sup> a plausible mechanism for the oxidation of lignin model compound **a** was proposed (Scheme 2a). In the first step, the *tert*-butoxyl radical forms from TBHP to initiate the reaction, which could as well further decompose to acetone and methyl radicals.<sup>[14]</sup> Meanwhile, LCN reacts with TBHP to afford LCN-OH, which contains active oxygen species at the carbon atoms neighbouring the graphitic nitrogen.<sup>[10]</sup> Then, the benzyl hydrogen, which is the least stable site of the substrate, gets abstracted by the *tert*-butoxyl radical to afford benzylic radicals and *tert*-butanol. The benzylic radicals convert to benzylic alcohol by OH transfer from LCN-OH, which concurrently regenerates the LCN catalyst. On repeating this step a dehydration reaction product **7** is formed. The above mechanism involves similar steps to the reported oxidation of alkyl-substituted aromatics with TBHP as oxidant.<sup>[6a,10]</sup> In the next step, the homolytic cleavage of **7** takes place at the aliphatic C<sub>α</sub>–O bond to form benzoyl and 2-methoxyphenoxy radicals, which have been trapped by TEMPO. Benzoyl radicals react with hydrogen radicals or methyl radicals in the next step, and the homolytic cleavage of **7** takes place at the aliphatic C<sub>α</sub>–O bond to form benzoyl and 2-methoxyphenoxy radicals, which have been trapped by TEMPO. Benzoyl radicals react with hydrogen radicals or methyl radicals to generate **1** and **2**, respectively, whereas 2-methoxyphenoxy radicals react with hydrogen radi-

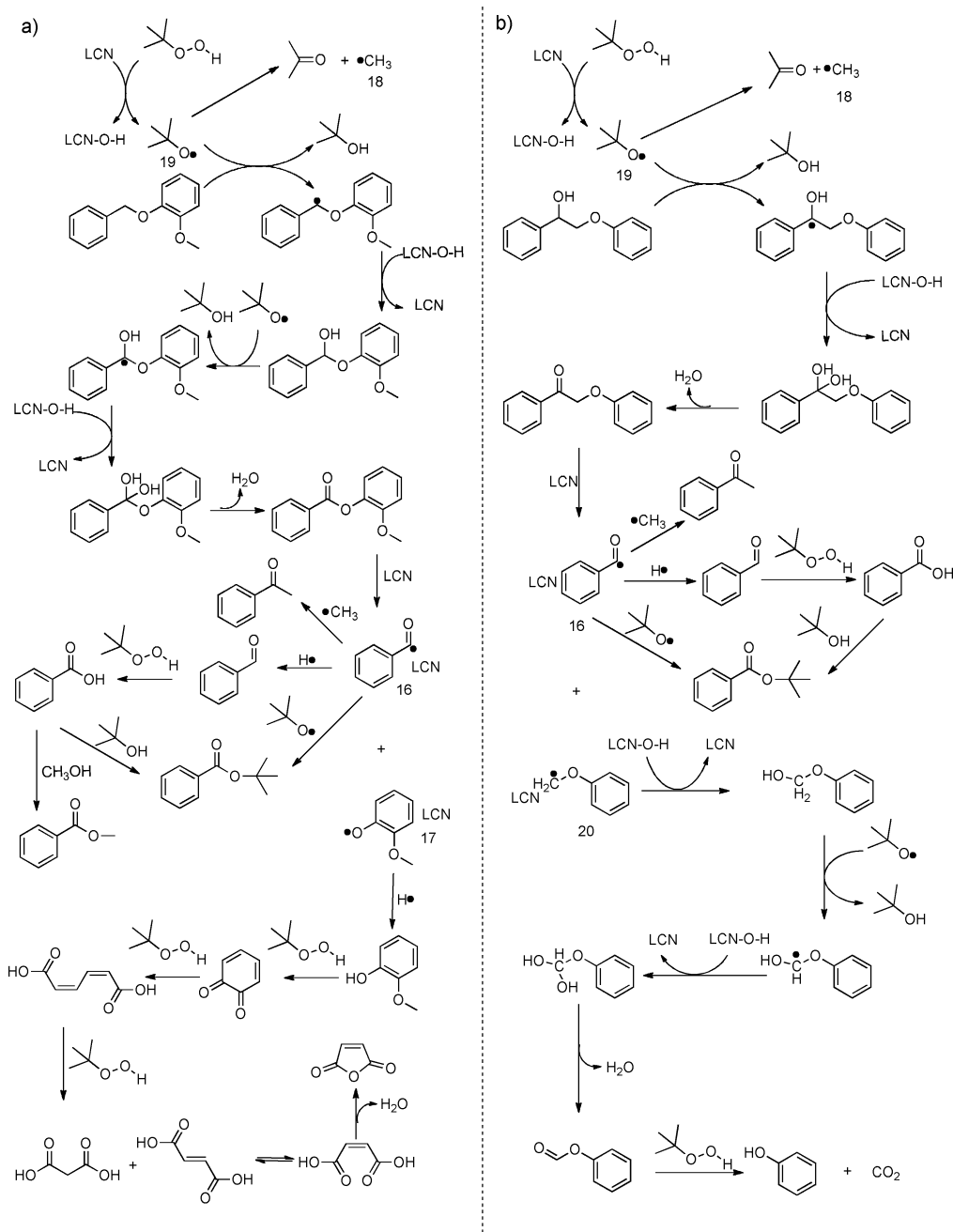
cals to produce **3**. In the presence of excess TBHP, **1** can be further oxidised to **4** whereas **3** decomposes to dicarboxylic acids and its derivatives in a similar manner to the Malaprade reaction. Besides, **4** can react with *tert*-butanol to form *tert*-butyl benzoate **5**.

With β-O-4 type lignin model compounds, the initiation step and reaction mechanism are similar to the case of **a**. In radical trapping experiments, **12**, **14**, **15** and **16** adducts were detected (see Scheme 1 and Figure S3), thus indicating that the homolytic cleavage happens at the C<sub>α</sub>–C<sub>β</sub> bond to afford benzoyl radicals and phenoxy methyl radicals. These radicals can be further converted to benzoic acid **4** and phenyl formate **8**. In the presence of excess TBHP, **8** can be converted to phenol **3** and carbon dioxide (Scheme 2b).

### Recycling experiment

A significant advantage of using LCN as the catalyst is its facile recovery. Evaluation of the long-term catalytic stability of LCN was undertaken at a reaction temperature of 120 °C employing **c** as the substrate. After one batch reaction, LCN was filtered out of the reaction mixture, washed and reused. Four batch reactions were performed without any further treatment. In the first run a high conversion of 85% was obtained with LCN. To our delight, the activity of LCN remains essentially constant in the second batch reaction and only decreases by about 5% in the fourth batch reaction (Figure 3a and Table S2). Interestingly, a change in product distribution was observed during the recycling experiments. For example, the yield of **4** decreased from 29.0 to 19.4 mol%, and correspondingly the yield of **11** (R<sub>1</sub>=R<sub>2</sub>=H) increased from 28.3 to 37.6 mol%, after four batch reactions. Considering **11** is formed through benzylic C–OH bond oxidation, whereas **4** is formed by C<sub>α</sub>–C<sub>β</sub> bond cleavage, it appears that the catalytic activity of LCN for the oxidation reaction was maintained upon recycling whereas the ability to break the C–C bond decreases gradually.

To shed light on structural/compositional changes of the catalyst during the recycling, XRD and XPS were used to characterise LCN after recycling. In the XRD pattern of LCN (Figure 3b), the peak at 2θ = 26.4° is attributed to reflection on the (002) planes of well-ordered graphene, which is very similar to the diffraction pattern of graphite. The shoulder peak at about 2θ = 30° and the broad hump at 2θ = 17° reflect the disordered state of graphene sheets.<sup>[15]</sup> LCN after reaction exhibits almost identical diffraction patterns to that of LCN, which suggests that the crystal structure of LCN does not change after recycling. According to the XPS spectra (Figure 3c,d), the nitrogen content in LCN after reaction decreased slightly from 6.2 to 5.4 wt% relative to fresh LCN. Nevertheless, curve-fitting analysis indicates that the content of graphitic nitrogen is still the predominant nitrogen species (3.3 wt%), similar to unused LCN, which explains the negligible decrease in catalytic activity during repeated oxidation reactions. Compared with fresh LCN samples, the oxygen content in used LCN increased significantly (from 3.5 to 14.4 wt%), not unreasonably though, as we propose the formation of LCN-OH between LCN and TBHP to be the first step in the reaction mechanism.



**Scheme 2.** Proposed mechanism of oxidative depolymerisation of a) a and b) c catalysed by LCN.

### Oxidation of birch wood lignin

We conducted preliminary studies employing the LCN-based catalytic system for the oxidation of organosolv lignin extracted from birch wood. Considering the more complex structure of real lignin, a higher temperature was employed (24 h, 12 equiv TBHP, 140 °C). Two fractions, that is, an orange oil fraction (45.8 wt%) and a brown solid fraction (33.6 wt%), were obtained after the reaction (Figure S5). The orange oil fraction is water soluble and obtained directly after filtration and freeze-drying. The brown solid fraction is obtained by extracting the remaining solid with ethanol. Both fractions were analysed by gel permeation chromatography (GPC; Figure S6) and

the results were compared with that of the starting material. The average molecular weight (MW) of the oil fraction is 4800, much lower than that of the starting material (MW 250000). The MW of the solid fraction is similarly small, despite exhibiting a wider MW distribution. GPC analysis indicates a significant depolymerisation of organosolv lignin over LCN in the presence of TBHP.

Figure 4 shows the FTIR spectra of the orange oil and the brown solid fractions, as well as of unreacted lignin. The IR spectra of the oil and the solid fractions are very different from that of the unreacted lignin. First, the intensities of the bands at 1713 and 1177  $\text{cm}^{-1}$  increase remarkably and a shoulder

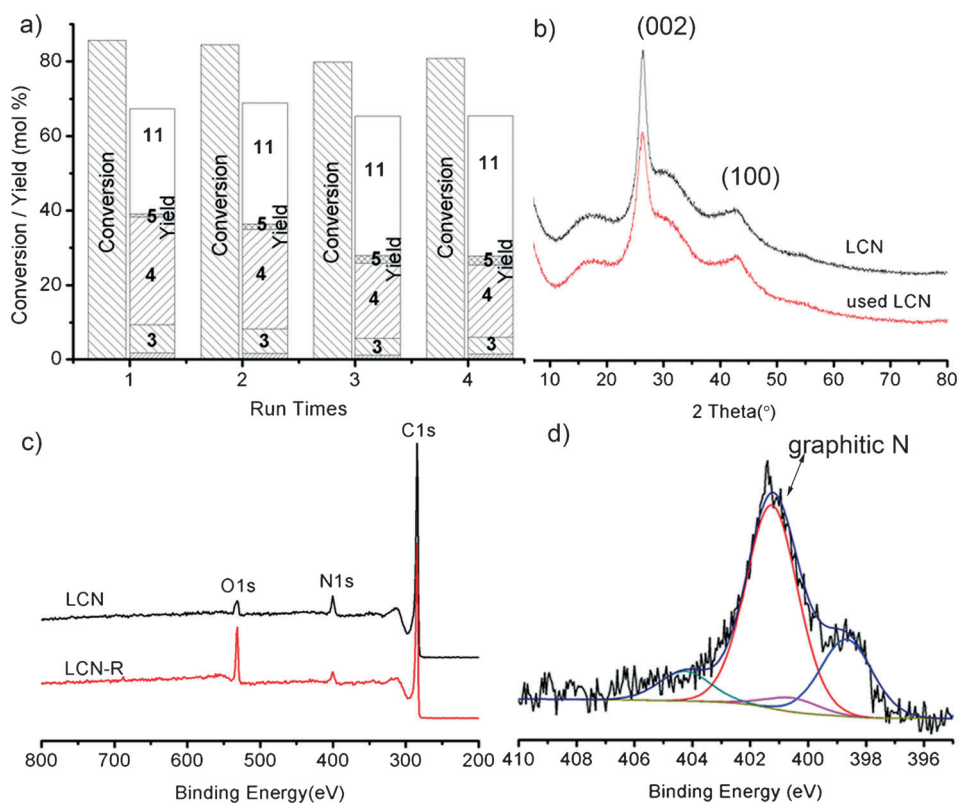


**Figure 3.** a) Conversion and product distributions of recycling experiments. Reaction conditions:  $\epsilon$  (0.5 mmol), TBHP (6.0 mmol, 70 wt% in water), LCN (0.01 g),  $\text{H}_2\text{O}$  (3 mL),  $120^\circ\text{C}$ , 12 h; the conversion and yield were determined by GC. b) XRD patterns and c,d) XPS spectra of LCN and used LCN.

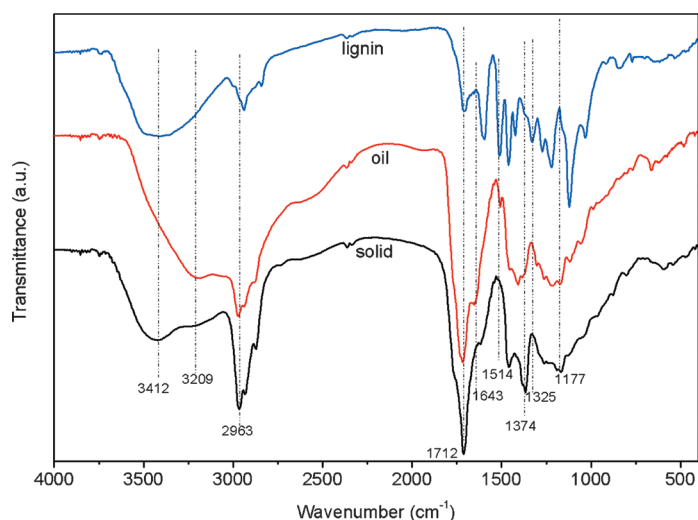


**Figure 4.** FTIR spectra of birch lignin and the oxidation products of birch lignin.

peak appears at approximately  $1643\text{ cm}^{-1}$  in the spectra of the products. The bands at  $1713$  and  $1643\text{ cm}^{-1}$  are attributed to non-conjugated and conjugated carbonyl stretching, respectively, and the band at  $1177\text{ cm}^{-1}$  is assigned to the carbonyl stretching of conjugated ester groups.<sup>[16]</sup> The changes indicate that an appreciable number of C–H and/or C–OH bonds in lignin are oxidised to C=O groups.<sup>[17]</sup> Besides, a portion of C–H

bonds in the  $\alpha$ -O-4 linkage in lignin are oxidised to C=O groups without C $_{\alpha}$ –O bond cleavage. As a result, it is evident that the oxidation of birch lignin occurs, thereby generating oxygen-enriched products. Second, a new band arises at about  $1374\text{ cm}^{-1}$  in the product spectra, which can be attributed to the phenolic hydroxyl group vibrations,<sup>[18]</sup> thus providing strong evidence of the cleavage of ether bonds in lignin. Furthermore, the intensity of the band at  $2963\text{ cm}^{-1}$  ascribed to C–H stretching vibrations in  $\text{CH}_3$  increases, whereas the bands at  $1514$  and  $1325\text{ cm}^{-1}$  ascribed to the aromatic ring and C–O stretching vibration in syringyl units decrease in the product spectra, which indicates that the aromatic structure and C–O bonds were partially decomposed.<sup>[19]</sup> The orange oil product seems to be more oxidised and its IR spectrum exhibits a stronger band at  $3209\text{ cm}^{-1}$  than the brown solid. More encouragingly,

$^{13}\text{C}$  NMR analysis of the oil fraction revealed the presence of small-molecule products (Figure S7). Overall, LCN exhibits similar catalytic behaviour in the oxidation of lignin model compounds and birch wood lignin, that is, it catalyses the oxidation of benzylic C–H and C–OH bonds into carbonyl groups, breaks the C $_{\alpha}$ –C $_{\beta}$  and C $_{\alpha}$ –O bonds, and further catalyses the decomposition of some unstable aromatic compounds. A blank experiment employing birch lignin with TBHP revealed that the structure of the lignin could be partly disrupted even without LCN, but to a lesser extent, which highlights the positive role of LCN in the oxidation depolymerisation of real lignin (see Figure S8 for FTIR analysis).

We further performed acid-catalysed hydrolysis with both fraction I (orange oil product) and fraction II (brown solid product) in ethanol–water solution at  $150^\circ\text{C}$ . For fraction I, diethyl succinate and other low-molecular-weight products (MW < 400, according to GC–MS spectra) were identified in GC–MS analysis.

For fraction II, diethyl succinate, diethyl phthalate and other low-molecular-weight products (MW < 400, according to GC–MS spectra) were obtained. Combined, 0.13 wt% of diethyl succinate and 0.75 wt% of diethyl phthalate were obtained. Notably, no such products were identified by GC–MS analysis by direct hydrolysis of birch lignin under the same hydrolysis conditions (see Figures S9–S11 for GC–MS spectra).

## Conclusion

By employing nitrogen-containing graphene material (LCN) as a catalyst and *tert*-butyl hydroperoxide as an oxidant, we systematically studied the oxidative decoupling of  $\alpha$ -O-4 and  $\beta$ -O-4 types of lignin model compounds in water. Under optimised conditions, high yields of monomeric products were obtained. The reaction follows a free-radical mechanism and the structures of key intermediates were identified by free-radical trapping experiments. Kinetic study and control experiments highlight that the key step for  $\alpha$ -O-4 model compound oxidation is the aliphatic C $_{\alpha}$ -O bond cleavage, whereas the key step for the  $\beta$ -O-4 type of lignin model compound is the cleavage of the C $_{\alpha}$ -C $_{\beta}$  bond. The LCN proved to be highly stable and could be used at least several times without appreciable decrease in activity.

This novel oxidative system can convert birch wood lignin into depolymerised products including a significant portion of liquefied product. These products may undergo further transformations more easily than untreated lignin. Further study is ongoing in our laboratory to enhance the yield of monomeric chemicals from real lignin.

## Experimental Section

### Chemicals

Potassium permanganate (KMnO<sub>4</sub>), sulfuric acid (H<sub>2</sub>SO<sub>4</sub>), barium chloride (BaCl<sub>2</sub>) and hydrogen chloride (HCl) were purchased from Beijing Chemical Industry Group Co., Ltd. 2-Bromoacetophenone, sodium nitrate (NaNO<sub>3</sub>), potassium carbonate (K<sub>2</sub>CO<sub>3</sub>), phenol, guaiacol, hydrogen peroxide (30 wt%, H<sub>2</sub>O<sub>2</sub>), *tert*-butyl hydroperoxide (70 wt% in water, TBHP) and 2,2,6,6-tetramethyl-1-piperidinyloxy (TEMPO) were purchased from Sigma-Aldrich. Natural flake graphite (99.99%) was purchased from Alfa Aesar. All these commercially available chemicals were used as received. 1-(Benzyloxy)-2-methoxybenzene (**a**), benzyl phenyl ether (**b**), 2-phenoxy-1-phenylethanol (**c**), 2-(2,6-dimethoxyphenoxy)-1-phenylethanol (**d**), 2-(2,6-dimethoxyphenoxy)-1-phenylethanol (**e**)<sup>[20]</sup> and organosolv lignin<sup>[21]</sup> were prepared by following literature procedures.

### Characterisation

Gel permeation chromatography (GPC) analysis was performed with a system equipped with a Waters 2410 refractive index detector, a Waters 515 HPLC pump and two Waters styragel columns (HT 3 and HT 4) with dimethylformamide as eluent at a flow rate of 1 mL min<sup>-1</sup> at 25 °C. The raw data were processed using narrow polystyrenes as calibrations on software Breeze. Fourier transform infrared (FTIR) spectroscopy was performed on a Bruker Equinox 55 infrared spectrometer. The number of scans was 16 with a resolution of 4 cm<sup>-1</sup> over the range of 4000–400 cm<sup>-1</sup>. Solid sample was finely mixed with KBr before pressing into a pellet for measurement. Oil sample was measured directly using KBr windows. Nuclear magnetic resonance (NMR) spectra were recorded on a Bruker 400, AV400 NMR spectrometer using [D<sub>6</sub>]dimethyl sulfoxide as the solvent. High-resolution transmission electron microscopy (HRTEM) images were taken on a Tecnai F30 (FEI) field-emission transmission electron microscope operated at an accelerating voltage of 300 kV. Scanning electron microscopy (SEM) images were obtained on

a JEM-6700F scanning electron microscope (JEOL). The sample was immobilised on a copper substrate by conductive adhesives without further processing. X-ray photoelectron spectroscopy (XPS) data were obtained on a VG ESCALAB MKII spectrometer, using a monochromated AlK $_{\alpha}$  X-ray source ( $h\nu = 1486.71$  eV, 5 mA, 15 kV). The data were converted into VAMAS file format and imported into the CasaXPS software package, calibrated by the C 1s signal (285.0 eV) and further processed. X-ray diffraction (XRD) was performed on a Bruker D8 advanced diffractometer using CuK $_{\alpha}$  ( $\lambda = 1.5406$  Å) radiation (40 kV, 30 mA cathodic current). Diffraction patterns were recorded within a  $2\theta$  range of 5–80° in a period of 32 min. Reaction products were analysed by gas chromatography (GC) and gas chromatography–mass spectrometry (GC–MS) on an Agilent 7890A gas chromatograph with a flame ionisation detector and an Agilent 7890A-5975 GC–MSD instrument, both equipped with HP-5 capillary columns (30 m  $\times$  250  $\mu$ m). In the oxidation of lignin, the solution of products was firstly frozen into ice in a fridge at –20 °C and then was freeze-dried on a Martin Christ Freeze Dryer with the vacuum at 0.31 mbar and ice condenser at –42 °C.

### Preparation of graphene oxide

In a first step, graphene oxide (GO) was synthesised according to a modified Hummer's method.<sup>[22]</sup> Briefly, natural graphite powder (5 g), sodium nitrate (5 g) and concentrated sulfuric acid (230 mL) were added to a flask placed in an ice bath. Then KMnO<sub>4</sub> (30 g) was added slowly to the mixture under vigorous stirring to avoid the temperature of the suspension exceeding 20 °C. The suspension was kept in the ice bath under stirring for 4 h, and was transferred into a water bath (35 °C) for 4 h under stirring. Afterwards, distilled water (460 mL) was added slowly to the suspension. The flask was transferred into a preheated oil bath for 4 h, with the temperature set at 98 °C. The reaction system was diluted with distilled water (1000 mL) followed by addition of H<sub>2</sub>O<sub>2</sub> solution (30%, 100 mL) to remove residual KMnO<sub>4</sub> and MnO<sub>2</sub>. The solid product was separated by filtration, washed repeatedly with 5% HCl solution until sulfate could not be detected by BaCl<sub>2</sub>, and finally washed with water to pH 7. The product was dried in an air oven at 60 °C for 120 h. Note, the major difference between this procedure and the original Hummer's method is that the duration of the three main steps, that is, in the ice bath (0 °C), water bath (35 °C) and oil bath (98 °C), in the synthesis is longer in this study to enable the graphene oxide to have the highest oxygen content.

### Preparation of nitrogen-containing graphene-based carbon

LCN was prepared in a two-step process from GO. In a first step, pyrolytic graphite oxide (PGO) was prepared through rapid heating of GO in a tube furnace under a hydrogen atmosphere. The heating started from room temperature at a heating rate of 20 °C min<sup>-1</sup> and was stopped once the temperature reached 800 °C. In a second step, the chemical vapour deposition (CVD) method was applied to prepare LCN from PGO and acetonitrile, which acted as the substrate and the nitrogen source, respectively. Acetonitrile was introduced into the CVD system by bubbling nitrogen gas (30 mL min<sup>-1</sup>) in acetonitrile at room temperature. The temperature of the oven was kept at 800 °C for 15 h.

### Catalytic reaction

Typically, the substrate (0.5 mmol), catalyst (0.01 g), oxidant and water (3 mL) were added in turn to a 35 mL glass reactor. After sealing with a Teflon lid, the reactor was placed into an aluminium block preheated at the designated temperature and kept at that temperature for a period of time. After that, the reaction vessel was cooled to room temperature. Cyclohexanone (0.05 g) was added to the system as internal standard and the system was extracted with ethyl acetate (2 mL×3). The organic phase was analysed by GC and GC–MS. The water phase was freeze-dried and characterised by GC, GC–MS, FTIR spectroscopy and NMR spectroscopy. For quantification, methanol (1 mL) was added to the solution together with 1,4-dioxane (0.010 g) as the internal standard, after which the solution was analysed by GC.

When birch lignin was used as the substrate, birch wood lignin (0.05 g), catalyst (0.01 g), TBHP (12.0 mmol, 70 wt% in water) and water (3 mL) were added in turn to a 35 mL glass reactor. After sealing with a Teflon lid, the mixture was heated to a designated temperature and kept at that temperature for a period of time. After that, the reaction vessel was cooled to room temperature. The solution was filtered and the filtrate was collected in a glass vial (water-soluble products, fraction I). The carbon catalyst was washed with ethanol and then isolated by filtration. The filtrate was collected into another vial (ethanol-soluble products, fraction II). Both fractions were freeze-dried and sent for further analysis, including GC, GC–MS, GPC and FTIR spectroscopy. In the acid-catalysed hydrolysis of the oxidation products of birch lignin, the substrate (either fraction I or II) was dissolved in ethanol (2 mL) and transferred into a glass tube (35 mL). Water (1 mL) and HCl (6 mmol) were added in turn. After sealing with a Teflon lid, the reactor was placed into an aluminium block preheated at 150 °C and kept at that temperature for 5 h. After that, the reaction vessel was cooled to room temperature. Cyclohexanone (0.02 g) was added to the system as an internal standard and the system was extracted with ethyl acetate (5 mL). The organic phase was analysed by GC and GC–MS.

### Recycling experiments

Recycling experiments were conducted at 120 °C using 2-phenoxy-1-phenylethanol (c) as the substrate. Other reaction conditions can be found in the section "Catalytic reaction". After reaction, the mixture was extracted with ethyl acetate (2 mL×3) and the organic phase was analysed by GC and GC–MS. The solution was filtered and the remaining solid (the catalyst) was washed with ethyl acetate, ethanol and water in turn and reused for the next batch of reactions under the same conditions.

### Free-radical trapping experiments

All free-radical trapping experiments were conducted at 80 °C. Other reaction conditions can be found in the section "Catalytic reaction". For  $\alpha$ -O-4 type model compound conversion, TEMPO (1 mmol) was added to the system after 5 min of reaction, after which the reaction continued for 55 min. For  $\beta$ -O-4 type model compounds, TEMPO (1 mmol) was added to the system 10 min after the reaction commenced, after which the reaction continued for 50 min. The reaction mixture was extracted with ethyl acetate (2 mL×3) and the organic phase was analysed by GC–MS.

### Acknowledgements

This study was financially supported by the A\*Star PSF project (WBS: R-279-000-403-305) and a MOE Tier-1 project (WBS: R-279-000-387-112).

**Keywords:** aromatic chemicals · graphene · heterogeneous catalysis · lignin · oxidation

- [1] a) G. W. Huber, S. Iborra, A. Corma, *Chem. Rev.* **2006**, *106*, 4044–4098; b) F. M. Kerton, Y. Liu, K. W. Omari, K. Hawboldt, *Green Chem.* **2013**, *15*, 860–871; c) X. Chen, S. L. Chew, F. M. Kerton, N. Yan, *Green Chem.* **2014**, DOI: 10.1039/c3gc42436g; d) N. Yan, P. J. Dyson, *Curr. Opin. Chem. Eng.* **2013**, *2*, 178–183.
- [2] a) F. G. Calvo-Flores, J. A. Dobado, *ChemSusChem* **2010**, *3*, 1227–1235; b) P. Azadi, O. R. Inderwildi, R. Farnood, D. A. King, *Renewable Sustainable Energy Rev.* **2013**, *21*, 506–523; c) T. Q. Yuan, F. Xu, R. C. Sun, *J. Chem. Technol. Biotechnol.* **2013**, *88*, 346–352; d) J. Zakzeski, P. C. A. Bruijninx, A. L. Jongerius, B. M. Weckhuysen, *Chem. Rev.* **2010**, *110*, 3552–3599; e) J. Wu, M. R. Rostami, E. S. Tzanakakis, *Curr. Opin. Chem. Eng.* **2013**, *2*, 17–25.
- [3] a) A. Toledano, L. Serrano, A. Pineda, A. A. Romero, R. Luque, J. Labidi, *Appl. Catal. B* **2014**, *145*, 43–55; b) M. D. Garrett, S. C. Bennett, C. Hardacre, R. Patrick, G. N. Sheldrake, *RSC Adv.* **2013**, *3*, 21552–21557; c) Q. Song, F. Wang, J. Cai, Y. Wang, J. Zhang, W. Yu, J. Xu, *Energy Environ. Sci.* **2013**, *6*, 994–1007; d) J. He, C. Zhao, J. A. Lercher, *J. Am. Chem. Soc.* **2012**, *134*, 20768–20775; e) N. Yan, C. Zhao, P. J. Dyson, C. Wang, L.-t. Liu, Y. Kou, *ChemSusChem* **2008**, *1*, 626–629; f) N. Yan, Y. Yuan, R. Dykeman, Y. Kou, P. J. Dyson, *Angew. Chem.* **2010**, *122*, 5681–5685; *Angew. Chem. Int. Ed.* **2010**, *49*, 5549–5553; g) J. Zhang, H. Asakura, J. v. Rijn, J. Yang, P. Duchesne, B. Zhang, X. Chen, P. Zhang, M. Saeyns, N. Yan, *Green Chem.* **2014**, DOI: 10.1039/c3gc42589d.
- [4] a) C. Z. Li, M. Y. Zheng, A. Q. Wang, T. Zhang, *Energy Environ. Sci.* **2012**, *5*, 6383–6390; b) S. Jia, B. J. Cox, X. Guo, Z. C. Zhang, J. G. Ekerdt, *ChemSusChem* **2010**, *3*, 1078–1084; c) T. Yoshikawa, S. Shinohara, T. Yagi, N. Ryumon, Y. Nakasaka, T. Tago, T. Masuda, *Appl. Catal. B* **2014**, *146*, 289–297; d) A. Toledano, L. Serrano, J. Labidi, *Fuel* **2014**, *116*, 617–624.
- [5] a) A. Azarpira, J. Ralph, F. Lu, *BioEnergy. Res.* **2014**, *7*, 78–86; b) T. Voilt, P. Rudolf von Rohr, *ChemSusChem* **2008**, *1*, 763–769; c) H. Lange, S. Decina, C. Crestini, *Eur. Polym. J.* **2013**, *49*, 1151–1173.
- [6] a) S. Kang, X. Li, J. Fan, J. Chang, *Renewable Sustainable Energy Rev.* **2013**, *27*, 546–558; b) Y. Zhao, Q. Xu, T. Pan, Y. Zuo, Y. Fu, Q.-X. Guo, *Appl. Catal. A* **2013**, *467*, 504–508.
- [7] a) M. P. Pandey, C. S. Kim, *Chem. Eng. Technol.* **2011**, *34*, 29–41; b) F. S. Chakar, A. J. Ragauskas, *Ind. Crop. Prod.* **2004**, *20*, 131–141; c) E. Adler, *Wood Sci. Technol.* **1977**, *11*, 169–218.
- [8] a) V. M. Roberts, V. Stein, T. Reiner, A. Lemonidou, X. Li, J. A. Lercher, *Chem. Eur. J.* **2011**, *17*, 5939–5948; b) S. Kundu, J. Choi, D. Y. Wang, Y. Choliy, T. J. Emge, K. Krogh-Jespersen, A. S. Goldman, *J. Am. Chem. Soc.* **2013**, *135*, 5127–5143; c) S. K. Hanson, R. T. Baker, J. C. Gordon, B. L. Scott, D. L. Thorn, *Inorg. Chem.* **2010**, *49*, 5611–5618.
- [9] A. Rahimi, A. Azarpira, H. Kim, J. Ralph, S. S. Stahl, *J. Am. Chem. Soc.* **2013**, *135*, 6415–6418.
- [10] Y. Gao, G. Hu, J. Zhong, Z. Shi, Y. Zhu, D. S. Su, J. Wang, X. Bao, D. Ma, *Angew. Chem.* **2013**, *125*, 2163–2167; *Angew. Chem. Int. Ed.* **2013**, *52*, 2109–2113.
- [11] S. H. Lim, H. I. Elim, X. Y. Gao, A. T. S. Wee, W. Ji, J. Y. Lee, J. Lin, *Phys. Rev. B* **2006**, *73*, 045402.
- [12] B. Sedai, C. Díaz-Urrutia, R. T. Baker, R. Wu, L. A. P. Silks, S. K. Hanson, *ACS Catal.* **2011**, *1*, 794–804.
- [13] E. Adler, S. Hernestam, *Acta Chemica Scandinavica* **1955**, *9*, 319–334.
- [14] L. Liao, Z. Song, Y. Zhou, H. Wang, Q. Xie, H. Peng, Z. Liu, *Small* **2013**, *9*, 1348–1352.
- [15] M. J. McAllister, J.-L. Li, D. H. Adamson, H. C. Schniepp, A. A. Abdala, J. Liu, M. Herrera-Alonso, D. L. Milius, R. Car, R. K. Prud'homme, I. A. Aksay, *Chem. Mater.* **2007**, *19*, 4396–4404.
- [16] J.-X. Sun, X.-F. Sun, R.-C. Sun, P. Fowler, M. S. Baird, *J. Agric. Food Chem.* **2003**, *51*, 6719–6725.

- [17] a) A.-P. Zhang, C.-F. Liu, R.-C. Sun, *Ind. Crop. Prod.* **2010**, *31*, 357–362; b) M. S. Jahan, D. A. Chowdhury, M. K. Islam, S. M. Moeiz, *Bioresour. Technol.* **2007**, *98*, 465–469.
- [18] R. Prado, X. Erdocia, J. Labidi, *Chemosphere* **2013**, *91*, 1355–1361.
- [19] a) O. Derkacheva, D. Sukhov, *Macromol. Symp.* **2008**, *265*, 61–68; b) Y. Sun, X. Qiu, Y. Liu, *Biomass Bioenergy* **2013**, *55*, 198–204.
- [20] J. M. Nichols, L. M. Bishop, R. G. Bergman, J. A. Ellman, *J. Am. Chem. Soc.* **2010**, *132*, 12554–12555.
- [21] L.-T. Liu, B. Zhang, J. Li, D. Ma, Y. Kou, *Acta Phys. Chim. Sin.* **2012**, *28*, 2343–2348.
- [22] W. S. Hummers, R. E. Offeman, *J. Am. Chem. Soc.* **1958**, *80*, 1339–1339.

---

Received: December 31, 2013

Revised: March 3, 2014

Published online on April 1, 2014